APPROX -mutual approximations between the Galilean moons: the 2016-2018 observational campaign

B. Morgado, R. Vieira-Martins, M. Assafin, D I Machado, J. I B Camargo, R Sfair, M Malacarne, F. Braga-Ribas, Vincent Robert, T Bassallo, et al.

Monthly Notices
of the
ROYAL ASTRONOMICAL SOCIETY

MNRAS **482,** 5190–5200 (2019) doi:10.1093/mnras/sty3040

APPROX – mutual approximations between the Galilean moons: the 2016–2018 observational campaign

B. Morgado,[1,2]★ R. Vieira-Martins,[1,2,3] M. Assafin,[2,3] D. I. Machado,[4,5] J. I. B. Camargo,[1,2] R. Sfair,[6] M. Malacarne,[7] F. Braga-Ribas,[1,2,8] V. Robert,[9,10] T. Bassallo,[1] G. Benedetti-Rossi,[1,2] L. A. Boldrin,[6] G. Borderes-Motta,[6] B. C. B. Camargo,[6] A. Crispim,[8] A. Dias-Oliveira,[1,11] A. R. Gomes-Júnior,[2,3,6] V. Lainey,[10,12] J. O. Miranda,[7] T. S. Moura,[6] F. K. Ribeiro,[7] T. de Santana,[6] S. Santos-Filho,[2] L. L. Trabuco,[5] O. C. Winter[6] and T. A. R. Yamashita[6]

Affiliations are listed at the end of the paper

Accepted 2018 November 5. Received 2018 November 5; in original form 2018 September 24

ABSTRACT

The technique of mutual approximations accurately gives the central instant of the maximum apparent approximation of two moving natural satellites in the plane of the sky. This can be used in ephemeris fitting to infer the relative positions of satellites with high precision. Only mutual phenomena – occultations and eclipses – can achieve better results. However, mutual phenomena only occur every six years in the case of Jupiter. Mutual approximations do not have this restriction and can be observed at any time in the year as long as the satellites are visible. In this work, we present 104 central instants determined from the observations of 66 mutual approximations between the Galilean moons carried out at different sites in Brazil and France during the period 2016–2018. For 28 events, we have at least two independent observations. All telescopes were equipped with a narrow-band filter centred at 889 nm with a width of 15 nm to eliminate the scattered light from Jupiter. The telescope apertures ranged between 25 and 120 cm. For comparison, the precision of the positions obtained with classical CCD astrometry is about 100 mas, for mutual phenomena it can be 10 mas or less, and the average internal precision obtained with mutual approximations is 11.3 mas. This new type of simple, yet accurate, observations can significantly improve the orbits and ephemeris of Galilean satellites and thus it can be very useful for the planning of future space missions to the Jovian system.

Key words: methods: data analysis – astrometry – planets and satellites: individual: Callisto – planets and satellites: individual: Europa – planets and satellites: individual: Ganymede – planets and satellites: individual: Io.

1 INTRODUCTION

Orbital studies of natural satellites can give us hints about the formation processes of moons (Charnoz et al. 2011; Crida & Charnoz 2012). They can also give us valuable information about the interiors of moons, with accurate estimations of the tidal effect. One example is the thermal equilibrium in Io (the innermost of the Galilean moons), determined by the agreement between the orbital energy loss and the heat evacuated at Io's surface (Lainey et al. 2009).

Any improvement of the orbits in these studies requires systematic astrometry of these moons, preferably over extended periods of time and, as much as possible, with accurate and precise measurements. These measurements, observables in a more general sense, are fitted with the use of dynamical models (De Sitter 1928; Lieske 1987; Lainey et al. 2009). For instance, an improvement in the study of the tidal force in the Jovian system requires positions with a precision better than 30 mas (Lainey 2016).

Usual CCD astrometry relies on the imaging of the target in the field of view (FOV) with an adequate number of catalogued

★ E-mail: morgado.fis@gmail.com

reference stars. For the Galilean moons, this is not an easy task. Jupiter's brightness (magnitude in the V band of around -2.5) makes it difficult to image catalogued stars ($V = 12$–20), as Jupiter saturates and spreads its light all over the FOV with longer exposures. Methods to reduce this brightness have been tried, but the precision in the classical CCD astrometry of a single satellite is yet not satisfactory (i.e. the standard deviation of ephemeris residuals from a few hundred observations per night ranges between 100 and 150 mas; Kiseleva et al. 2008).

Mutual occultations and eclipses provide very precise relative positions between two satellites. The drawback is that they can only be observed during the equinox of the host planet, when the Earth and the Sun pass through the orbital plane of the satellites. In the case of Jupiter, this occurs every 6 yr, for Saturn every 15 yr and for Uranus every 42 yr (Arlot et al. 2012, 2013, 2014). For the Galilean satellites, mutual phenomena can deliver relative positions with a precision better than 5 mas (Emelyanov 2009; Dias-Oliveira et al. 2013). More than 600 light curves were obtained in the last mutual phenomena campaign (called PHEMU15) between the Galilean moons, with an average precision of 24 mas (Saquet et al. 2018).

This scenario motivated the search for alternative methods to obtain astrometric data for these satellites. For example, Peng et al. (2012a) determined the relative positions between a pair of satellites when they are close together in the FOV, with a relative distance smaller than 85 arcsec, and they obtained precisions of 30 mas in these relative positions.

A more recent attempt is the mutual approximations technique that we have developed (Morgado et al. 2016), first suggested by Arlot et al. (1982). In this method, the instant of the maximum apparent approximation in the sky plane between two moving satellites can be determined with a precision that corresponds to less than 10 mas. The technique solves two problems in the CCD astrometry of the Galilean moons: the determination of the pixel scale and the orientation of the CCD with respect to the right ascension and declination axes in the sky (Emelyanov 2017). Also, it is easy to perform observations using this technique with telescopes that have a small aperture size (of a few centimetres). One important aspect of the method is the correct registering of time. Fortunately, this is also usually easy to accomplish with GPS receivers, specialized software or Internet services that calibrate the acquisition computer's UTC time inserted in the images.

In this paper, we give details of APPROX, an observational campaign of mutual approximations between the Galilean moons. It is a collaboration between Brazilian and French institutes, with six observational sites. This campaign observed 66 mutual approximations, obtaining 104 distance curves between 2016 February and 2018 August. The average precision of the central instant was 11.4 mas using the relative velocity in each event to convert between seconds of time and arcseconds. We also present a procedure to use the mutual approximation data as observables to determine the parameters of the satellites' orbits in ephemeris fitting.

In Section 2, we give an overview of the mutual approximation method. In Section 3, we describe the observational campaign, prediction, simulations and observations, and we explain how we processed the observed data. In Section 4, we present our results. In Section 5, we describe a procedure to use the central instants of mutual approximations for ephemeris fitting. We give our conclusions in Section 6.

2 THE METHOD OF MUTUAL APPROXIMATIONS

A detailed description of the method of mutual approximations has been given in Morgado et al. (2016). Here, we briefly summarize the principles of this method.

It is possible to determine the International Celestial Reference System position of a target in a CCD frame but an astrometric star catalogue is required to find the pixel scale, the CCD orientation and the zero point. The zero point is not needed when fitting ephemeris of natural satellites if the relative distances are known.

However, in the case of the Galilean satellites, it is not trivial to determine the pixel scale and image orientation without catalogue reference stars. One possibility is to use the measured relative satellite positions and motions and a reference ephemeris as a template (Peng et al. 2012a), but then the 'true' relative distances might be masked by the correlation with the errors in the ephemeris scale and orientation.

In the mutual approximation technique, we do not work with scaled distances, but with instrumental distances given pixel units. Scaled distances can be derived, but are not used in any fitting for finding the central instant and impact parameter and their errors – only instrumental distances are used for that. We can derive the pixel scale and CCD orientation using an ephemeris as a template, or we can use the nominal pixel scale of the instrument, but only for internal checking purposes (e.g. converting the impact parameter and its uncertainties to milliarcseconds in order to have a better evaluation of the fit). We emphasize that post-derived scaled distances between the satellites are not the primary result of the method of mutual approximations.

Thus, the main result of the method is the central instant at the maximum apparent approximation between two satellites, so we must calibrate time correctly, preferably with a precision better than 0.1 s. We do this using GPS receivers or by using the time-calibration software called Dimension 4.[1]

The mutual approximation method consists of fitting the apparent distances s_{ij} in the sky plane between two moving satellites i and j by a N-degree polynomial in time, defined by

$$s_{ij}^2(t) = \sum_{n=1}^{N} a_n\, t^n. \tag{1}$$

The underlying assumption that actually defines a mutual approximation is the assumption that s_{ij} gradually decreases with time, reaches a minimum and then starts to increase. The use of the square of s_{ij} simplifies computations. The degree of the polynomial is determined by evaluating tentative fittings to the (squared) apparent distances computed from a reference ephemeris.

We then use the fitted polynomial coefficients (a_n) to determine the central instant t_0 (the instant at maximum approximation, when the apparent distance is minimum), the impact parameter d_0 (the minimum apparent distance in the sky plane between both satellites, which occurs by definition at t_0 when the approximation is at maximum), the relative velocity v_0 at t_0 between both satellites in the plane of the sky, and their uncertainties (σd_0, σt_0 and σv_0). The central instant is always obtained in UTC. When fitting observations, the impact parameter and its uncertainty are obtained in pixels, and the relative velocity and its uncertainty in pixels per second of time. When fitting reference ephemeris data, the impact parameter

[1] See http://www.thinkman.com/dimension4/.

is generally computed in arcseconds and the relative velocity in arcseconds per second of time.

We also correct a shift in the observed central instant due to effects on the apparent distances caused bythe following: the different apparent sizes of each satellite and the solar phase angle correction; the atmospheric refraction; the diurnal and annual aberration. The correction is determined after comparing the shift in the central instant obtained from fittings using a reference ephemeris with and without these effects. The shift is usually in the range 1–6 s (5–30 mas).

Marks in the surface, or topography, of the satellites could affect the centroid measurement. As pointed out by Lindegren (1977), the maximum offset could be 35 mas, and would affect systematically all astrometric measurements during a run. Only a very precise albedo map of these satellites in the spectral region of the observations (in our case, 889 nm) would allow us to infer its contribution exactly. However, we highlight that, for mutual approximations, we would be affected only by a fraction of this offset, along the direction of relative motion between both satellites.

After all the fittings and computations of all parameters, for analysis and comparison purposes, we only use non-squared apparent distances. Once ordered in time, we have the distance curves of the event. There are two types of observed distance curves (i.e. measured and fitted) and two types of ephemeris distance curves (i.e. ephemeris- and fitted-based). The nature of the distance curves discussed in the text should be clear from the context.

3 OBSERVATIONAL CAMPAIGN

An observational campaign starts with the prediction of the apparent close approximations between two satellites that are really interesting. The second step is the simulation of these events, which can give some hints about the best instrumental configuration and observation procedures for the participants of the campaign. The third step is the observation itself, and the final step is the analysis of the data acquired.

3.1 Prediction

The predictions of the approximations were made with the topocentric ephemeris for each participating observatory using NASA's Navigation and Ancillary Information Facility (NAIF) SPICE[2] toolkit, Jovian ephemeris JUP310 and planetary ephemeris DE430.

The precision premium (Peng et al. 2008) predicts an increase in the precision in the measurement of apparent distances between two objects in the plane of the sky when this distance is smaller than 85 arcsec. In this scenario, we avoid the effects of distortions in the FOV, as both satellites should be affected in the same way. In order to avoid a prohibitive number of events, we only choose the approximations with an impact parameter smaller than 30 arcsec.

We selected all the mutual approximations that were visible for the observatories with an elevation above 30°. We set a minimum apparent distance of 10 arcsec between both satellites and the Jupiter limb. In total, we predicted 102 events between 2016 February and 2018 August. From these, we observed 66 mutual approximations; the others were lost as a result of bad weather conditions or instrumental issues.

[2]See http://naif.jpl.nasa.gov/naif/.

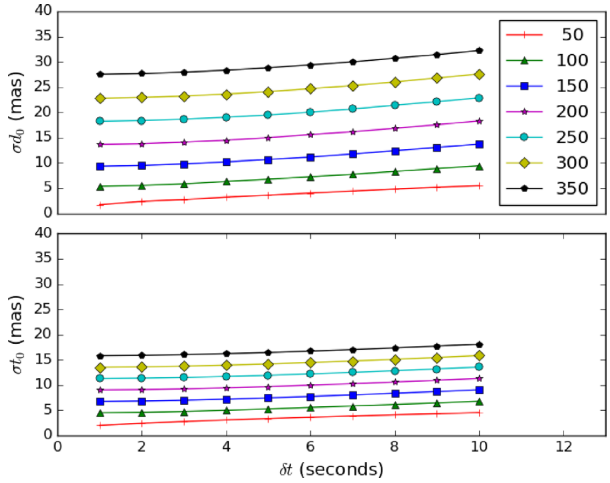

Figure 1. Simulating the observation of a mutual approximation with different values for the S/N (S/N - σ_{noise}) and time resolution (δt); the x-axis is δt, the upper y-axis is the error of the impact parameter (σd_0) and the lower y-axis is the error of the central instant (σt_0), both in mas. The different colours and marks represent different $\sigma_{\rm noise}$ regimes, in mas.

3.2 Simulations

In order to test the feasibility of the selected events, it is important to simulate observations and to analyse the different aspects that arise in each scenario. First, we study the expected precision of the mutual approximation's central instant (σt_0) and impact parameter (σd_0) for different values of time resolution (δt) and signal-to-noise ratio (S/N). Secondly, we evaluate the ideal duration of the observation of a mutual approximation. Thirdly, we mimic the presence of gaps in the distance curve, which are often caused by bad weather conditions or instrumental issues.

Let us illustrate all three steps in the simulation of events by taking as an example an approximation between Io (501) and Ganymede (503), which occurred on 2016 February 24. We added a Gaussian error with standard deviation equal to $\sigma_{\rm noise}$ in the distance between the pair of satellites to simulate real observations. We repeated the simulation 100 times with normalization to remove random systematic errors.

In the first step, we studied how the central instant and impact parameter errors are affected by different S/N and different δt (the time difference between two consecutive images). It is clear that the best-case scenario is a high S/N and a low δt. However, part of the time resolution is related to the time exposure, which in turn is correlated with the S/N. Thus, the simulations in this step show us which parameter we must prioritize to obtain the best results.

For the simulations in this step, we chose δt ranging between 1.0 and 10.0 s and $\sigma_{\rm noise}$ between 50 and 350 mas. The result is displayed in Fig. 1 where we can see that a high $\sigma_{\rm noise}$ (low S/N) affects the precision of the impact parameter (σd_0) and the central instant (σt_0) more than the time resolution itself. This means that a good S/N should be prioritized in the observations. For the remaining simulations, we used $\delta t = 4$ s and $\sigma_{\rm noise} = 100$ mas, which are the mean values in Morgado et al. (2016).

In the second step, the simulations can be used to evaluate the duration for which a mutual approximation should be observed. We simulate observations starting 1 h before and ending 1 h after the central instant (t_0). We eliminated pairs of simulated images

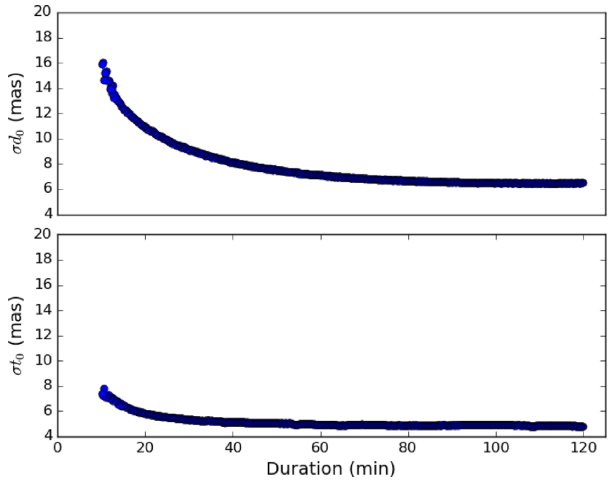

Figure 2. Simulating the duration of the mutual approximation event; the x-axis is the duration of the event (Δt), symmetrical with regard to the central instant (t_0); the upper y-axis is the error of the impact parameter (σd_0) and the lower y-axisis the error of the central instant (σt_0), both in mas.

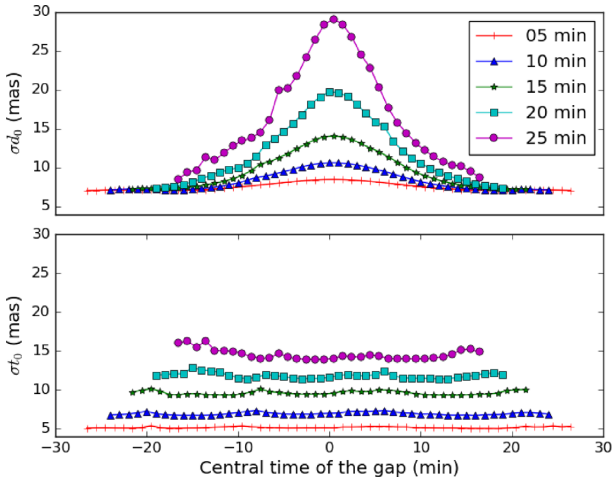

Figure 3. Simulating gaps in a mutual approximation; the x-axis is the central time of the gap $t_{\rm gap}$, the upper y-axis is the error of the impact parameter (σd_0) and the lower y-axis is the error of the central instant (σt_0), both in mas. The different colours and marks represent different sizes of the gap in minutes.

symmetrically placed around the central instant, one pair at a time, until our model failed to determine the central instant. This happens for Δt smaller than 10 min (5 min for each side around t_0).

As seen in Fig. 2 for events with a duration between 120 and 40 min, there is no significant difference in the precision of the result obtained for the central instant. For the next simulations, we used distance curves of 60 min with 30 min before and after the central instant.

In the third step, the simulations mimic problems that arise from instrument issues and/or bad weather conditions, in order to evaluate how the absence of points along the curve affects the error of the results. The simulations are divided into two different scenarios: (i) gaps are present along the whole curve; (ii) only one side of the curve is available. Both scenarios were explored in Morgado et al. (2016), but here we study them in detail.

In the first scenario, it is not only the size of the gap that matters, but also the gap location. We explored gaps with sizes $\Delta t_{\rm gap}$ equal to 5, 10, 15, 20 and 25 min, in different positions along the distance curve with respect to the central time of the gap $t_{\rm gap}$. In Fig. 3, we plot the errors of the impact parameter (σd_0) and the central instant (σt_0) over $t_{\rm gap}$. We remark that the location of the gap does not affect σt_0, whereas σd_0 is strongly affected by gaps near the central instant. This type of gap always occurs during the period of mutual phenomena when the mutual approximation culminates in an occultation, during which it is not possible to measure the (x,y) centroids of both satellites individually.

The distance curve in a mutual approximation should naturally be a quasi-symmetrical curve with respect to the central instant. Thus, observing only one side of the curve precludes a good determination of the central instant. In the second scenario, we investigated how close to the central instant we can start (or finish) one observation and still obtain good precision. In the simulations, one by one, we eliminate points only from one side of the curve and we compute the errors in the impact parameter (σd_0) and the central instant (σt_0). The results can be seen in Fig. 4, which shows that the central instant error is strongly affected by the absence of only one side of the curve. For observations starting less than 5 min before the central instant, the error can be up to 30 mas or more.

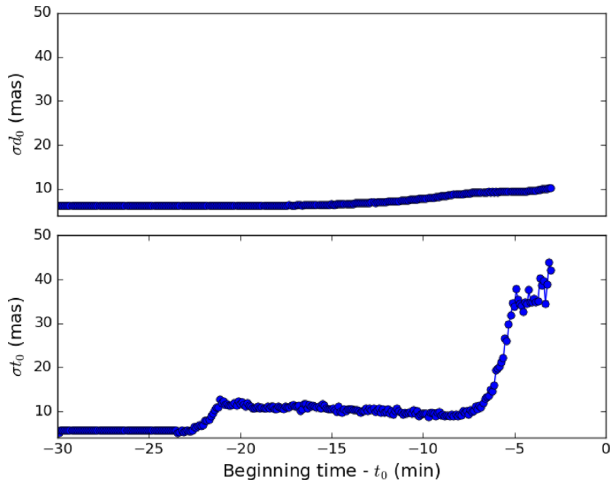

Figure 4. Simulating one-sided curves in a mutual approximation; the x-axis is the beginning time minus the central instant in minutes; the upper y-axis is the error of the impact parameter (σd_0) and the lower y-axis is the error of the central instant (σt_0), both in mas.

The first and second steps of simulations show us the eventual limitations of the method for each event. They allow us to alert observers to take the necessary precautions in their instrumental set-up and observational strategies. This optimizes the outputs of each event and ultimately improves the overall results of the campaign. The two scenarios in the third step of simulations show us what to expect in the realistic case of a mutual approximation event with bad weather conditions and/or instrument issues. It is worth noting that even in the worst-case scenarios with errors greater than 30 mas, the measurements can still be very useful in the ephemeris fitting of the Galilean satellites.

3.3 Observations

The observations were made at five different sites in the south and south-east of Brazil and one site in the south-east of France. The

Table 1. Observation information for the 2016–2018 mutual approximations campaign.

Site Alias MPC code	Longitude Latitude Altitude	Team of observers	Telescope aperture CCD Pixel scale	Number of events detected
Itajubá/MG-Brazil OPD 874	45°34′57.″5 W 22°32′07.″8 S 1864 m	B. Morgado J. I. B. Camargo T. Bassallo A. R. Gomes-Júnior S. Santos-Filho A. Dias-Oliveira G. Benedetti-Rossi	60 cm Andor/Ikon 0.37 arcmin px^{-1}	29
Foz do Iguaçu/PR-Brazil FOZ X57	54°35′37.″0 W 25°26′05.″0 S 184 m	D. I. Machado L. L. Trabuco	28 cm Raptor/Merlin 0.73 arcmin px^{-1}	35
Guaratinguetá/SP-Brazil FEG XXX	45°11′25.″5 W 22°48′05.″5 S 543 m	R. Sfair T. de Santana L. A. Boldrin G. Borderes-Mota T. S. Moura T. Akemi B. C. B. Camargo O. C. Winter	40 cm Raptor/Merlin 0.55 arcmin px^{-1}	24
Vitória/ES-Brazil GOA XXX	40°19′00.″0 W 20°17′52.″0 S 26 m	M. Malacarne J. O. Miranda F. Krieger	35 cm SBIG/ST-8X-ME 0.65 arcmin px^{-1}	8
Curitiba/PR-Brazil UTF XXX	49°11′45.″8 W 25°28′24.″6 S 861 m	F. Braga-Ribas A. Crispim	25 cm Watec/910HX 0.32 arcmin px^{-1}	5
Haute de Province/France OHP 511	05°42′56.″5 E 43°55′54.″7 N 633 m	V. Robert V. Lainey	120 cm Andor/CCD42-40 0.38 arcmin px^{-1}	3

geographical longitude, latitude, altitude and the Minor Planet Center (MPC) observatory code of the sites (XXX for sites without a code) for each observatory are listed in Table 1, which also displays instrumental information for each site, the observers and the number of positive detections. Note that the aperture diameters of the telescopes ranged between 25 and 120 cm.

We encouraged the coverage of each event by multiple sites not only in order to lose as few events as possible due to bad weather conditions or instrumental problems, but also because of the advantage gained in the analysis. Also, we proposed that the observers place the satellites of the mutual approximation in the central part of the CCD FOV to attenuate the effects of field distortions, if any (see Peng et al. 2012b).

All the observations were made with a narrow-band filter centred at 889 nm with a width of 15 nm. Radiation in this spectral range is absorbed by the methane in Jupiter's high clouds, making its albedo drop to values below 0.1 (Karkoschka 1994, 1998). This filter is very efficient in decreasing the scattered light of Jupiter without affecting the brightness of the satellites, as pointed out by Karkoschka (1994). Thus, we could obtain good S/N images of the satellites ($V \sim 5$) with exposures of a few seconds without the interference of the scattered light of the planet.

3.4 Data processing

The majority of the observations were acquired in FITS format with the time registered in the header. The UTF site recorded observations with a video camera with the time stamped in each frame. The conversion from AVI to FITS and the time extraction were performed with the AUDELA[3] software. The processing of the FITS images was done in three steps.

First, all images were corrected for bias, dark and flat-field using standard IRAF[4] procedures (Butcher & Stevens 1981).

The second step was the determination of the satellite's (x,y) centres in the images using the PRAIA package (Assafin et al. 2011). This package measures the object's centroid with a two-dimensional circular symmetric Gaussian fit over pixels within one full width at half-maximum (FWHM = seeing) from the centre. The average error of the centroid measurement was 1/20 of a pixel. Using the nominal pixel scale of the instruments, this translates to errors in the range of 16–36 mas.

[3]See http://audela.org/.
[4]See http://iraf.noao.edu/.

The third step was the application of the mutual approximation method itself, described in Section 2. We fitted the observed and ephemeris distance curves for the determination of auxiliary ephemeris central instants of time, impact parameter and relative velocities. After the corrections for solar phase angle, atmospheric refraction, diurnal and annual aberration, we obtained the final observed central instants, as well as the observed impact parameters and relative velocities, and their errors. It turned out that a fourth-degree polynomial was used to fit all the distance curves. A Python-based software (Robitaille et al. 2013) was specially developed for performing all the computations of this step.

Thus, at the end of the data processing, we obtained the central instant of the maximum apparent approximation (t_0) between both satellites, their impact parameter (d_0), their relative velocity (v_0) at t_0, also in the plane of the sky, and the errors for all these parameters. Without any scaling, d_0 and v_0 (and their errors) are measured in pixels and pixels per second.

4 RESULTS

The 2016–2018 observational campaign reported in this paper started in 2016 February and ended in 2018 August. A total of 66 events were successfully observed. For 28 mutual approximations, simultaneous observations were made at two or more sites. In total, 104 independent observations were obtained.

The multiple coverage observational strategy reduced the number of events lost because of bad weather conditions or instrumental issues. An extreme example was the event between Io and Europa on 2016 April 19. This approximation was observed by five sites: OPD, FOZ, GOA, UTF and OHP. Fig. 5 contains the distance curves obtained by each observatory. For comparison, we used the nominal pixel scale (Table 1) for each site to transform the apparent distance in the plane of the sky from pixels to arcsec. The differences between the observations and the ephemeris JUP310 from JPL[5] were −0.2, −4.8, −7.8, −0.5 and −5.5 mas and the precision was 3.8, 8.2, 8.2, 12.0 and 5.6 mas, respectively. These observations combined represent an offset of −3.8 mas with a standard deviation of 2.9 mas.

The results of this campaign can be found in Tables 2 and 3, which contain the date of the event and the satellite pairs in the form S_iAS_j, where 501 stands for Io, 502 for Europa, 503 for Ganymede and 504 for Callisto. We provide the sites involved in each observation (using the alias defined in Table 1). For each site, we give the obtained central instant (t_0) and its uncertainties (σt_0) in seconds of time and in mas, respectively, and the difference between the observed central instant and that determined by using the (topocentric) ephemeris JUP310 with DE435 (Δt_0), in seconds of time and in mas. All times are UTC. In the last column, we have the label N of each mutual approximation, which is a sequential number following the chronological order of the events. Table 2 displays the results of the 48 distance curves obtained in 2016 and Table 3 shows the results of the 25 and 31 curves observed in 2017 and in 2018, respectively.

Our results are also illustrated in Fig. 6, which displays central instant offsets in mas with respect to the JUP310 ephemeris (dashed line at zero offset) for each mutual approximation. The different colours represent different sites and the dotted line is the difference between the NOE-5-2010-GAl.a and JUP310 ephemeris. The rms between our observations and the JUP310 and NOE-5-2010-GAl.a ephemeris were 14.4 and 18.2 mas, respectively.

According to Tables 2 and 3, very few observations had central instants with internal errors worse than the ideal 30 mas suggested in Lainey et al. (2009) and Lainey (2016) for an effective contribution to the study of tidal forces in the Jovian system (i.e. nine observations out of 104, which is about 9 per cent). About 87 per cent (90 observations) had uncertainties below 20 mas and 65 per cent (67 observations) below 10 mas. One extreme example was the mutual approximation between Io and Callisto observed at OPD on 2016 April 12 ($N = 10$). The internal error was 8.9 s (51.6 mas). This event was heavily affected by bad weather, presenting a 20-min gap before the central instant, with observations having to stop just 15 min after the central instant (see Fig. 7). All observations with internal errors worse than about 20 mas were affected at some extent by bad weather conditions and/or instrumental issues, such as gaps in the curve or low S/N. These scenarios were predicted and explored in our simulations in Section 3.2.

5 EPHEMERIS FITTING PROCEDURE

In order to create an ephemeris, it is necessary to fit a dynamical model to the observations. In the case of natural satellites, the fitting is made by using the standard method of variational equations (see Lainey, Duriez & Vienne 2004a, Lainey, Arlot & Vienne 2004b). Here, we present a method for ephemeris developers that allows the addition of central instants from mutual approximations to ephemeris fitting, by the development of more adequate conditional equations to the problem.

In the case of mutual approximations, we should in principle solve for the partial derivatives $\partial t_0/\partial c_l$ to obtain the following conditional equation of the problem:

$$t_0^{\rm o} - t_0^{\rm c} = \Delta t_0 = \sum \frac{\partial t_0^{\rm c}}{\partial c_l} \Delta c_l. \tag{2}$$

Here, c_l represents each of the l parameters that we are fitting, usually the initial positions and velocities (X_0, Y_0, Z_0, $\dot{X}_0$, $\dot{Y}_0$, $\dot{Z}_0$) for each body in the integration, and other parameters such as the masses, J_2, J_4, etc., Δc_l represents the correction for each fitted parameter, $t_0^{\rm c}$ is the central instant computed by the dynamical model, $t_0^{\rm o}$ is the central instant obtained from the observations and the difference $t_0^{\rm o} - t_0^{\rm c} = \Delta t_0$ represents the 'observed minus computed' offset.

However, equation (2) cannot be solved analytically and a numerical approach consumes too much CPU time (see Emelyanov 2017). Fortunately, we can develop equivalent equations to the problem that are solvable.

Consider the apparent distance in the plane of the sky s_{ij} between two satellites i and j, where s_{ij} is minimum at the central instant t_0, that is, $({\rm d}s^{\rm o}/{\rm d}t)(t_0) = 0$. Knowing this, we can write

$$\frac{{\rm d}s^{\rm o}}{{\rm d}t}(t_0) - \frac{{\rm d}s^{\rm c}}{{\rm d}t}(t_0) = \sum \frac{\partial}{\partial c_l} \left[\frac{{\rm d}s^{\rm c}}{{\rm d}t}(t_0)\right] \Delta c_l, \tag{3}$$

where $({\rm d}s^{\rm c}/{\rm d}t)(t_0)$ is the value computed by the dynamical model, and the difference $({\rm d}s^{\rm o}/{\rm d}t)(t_0) - ({\rm d}s^{\rm c}/{\rm d}t)(t_0)$ also represents an 'observed minus computed' offset. Equation (3) is a more suitable conditional equation to the problem. It can be rewritten as follows.

The apparent distance s_{ij} between satellites i and j can be written as

$$s_{ij} = \sqrt{\Delta x_{ij}^2 + \Delta y_{ij}^2}, \tag{4}$$

[5] See http://www.jpl.nasa.gov/.

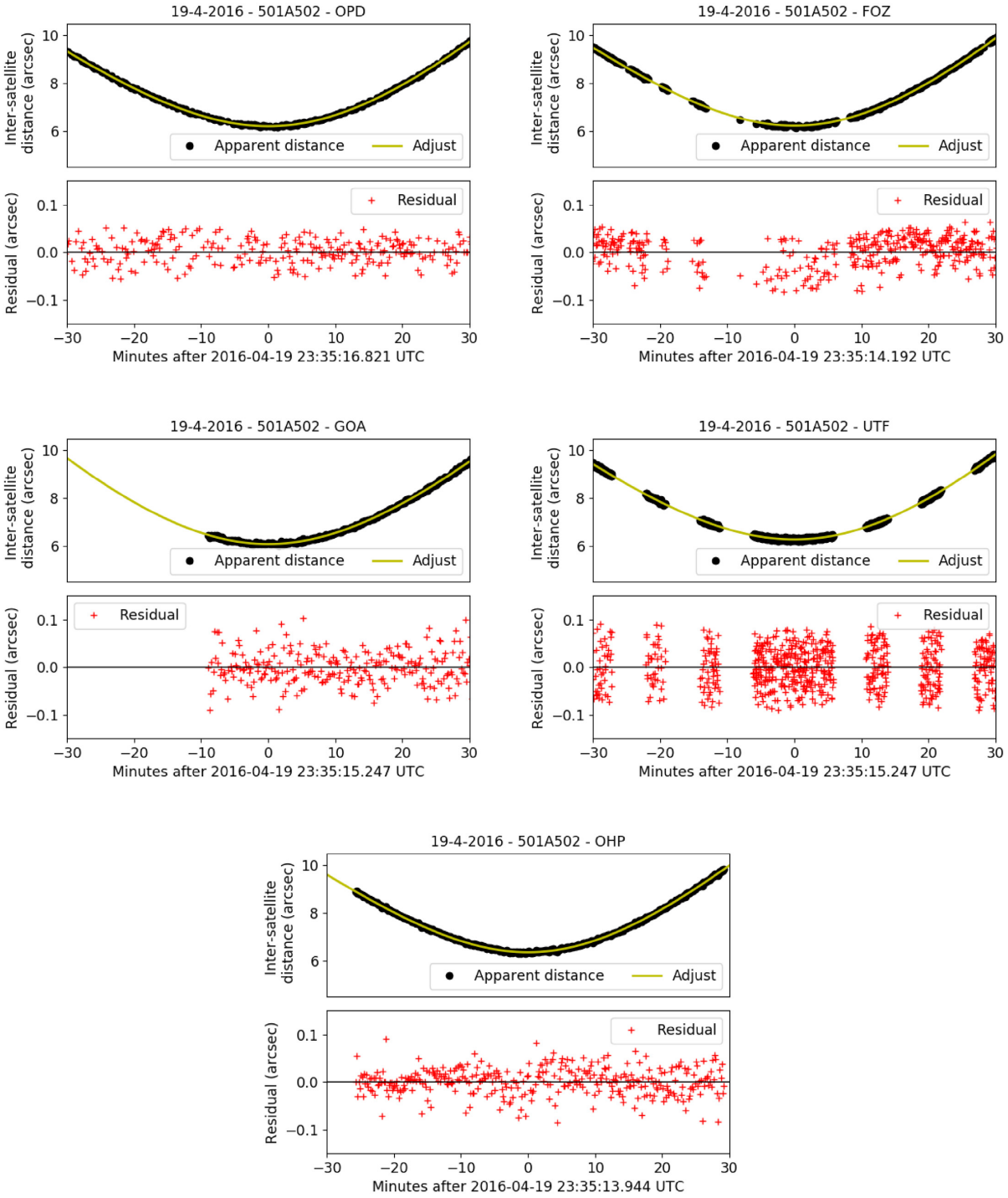

Figure 5. Curves of observed apparent distance in the plane of the sky between Io and Europa in the mutual approximation of 2016 April 19 for five sites: OPD, FOZ, GOA, UTF and OHP. Inter-satellite distances, d, are denoted by black dots and the model fit is shown by the yellow line. In the bottom panel, the red crosses are the residual of the fitting. We used the nominal pixel scale (Table 1) for each site to convert the apparent distances from pixels to arcsec.

with

$$\Delta x_{ij} \simeq (\alpha_i - \alpha_j)\cos(\delta_m), \tag{5}$$

$$\Delta y_{ij} \simeq \delta_i - \delta_j, \tag{6}$$

$$\delta_m = \frac{\delta_i + \delta_j}{2}, \tag{7}$$

where α_i and α_j are the satellites' right ascensions, δ_i and δ_j their declinations and δ_m is the mean declination of both satellites, which is the first-order polynomial approximation for gnomonic projection.

Table 2. Central instant: results of the mutual approximation campaign for 2016. Note that 501 stands for Io, 502 for Europa, 503 for Ganymede and 504 for Callisto. σt_0 is the central instant error in seconds of time and in mas (using the relative velocity in each event obtained with the ephemeris) and Δt is the comparison between the observation and the ephemeris JUP310 (with DE435) from the JPL in the sense of 'observation minus ephemeris' in seconds of time and in mas. N is a sequential number with time that labels each observed mutual approximation. Time is UTC.

Date (yy-mm-dd)	Event	Observer	t_0 (UTC) (hh:mm:ss.ss)	σt_0 (s)	σt_0 (mas)	Δt_0 (s)	Δt_0 (mas)	N
2016-02-03	502A503	OPD	04:48:01.1	4.2	30.4	+0.9	+6.3	1
2016-02-08	501A502	FOZ	06:29:38.4	0.6	2.6	+1.5	+6.8	2
2016-02-15	502A503	FOZ	08:39:28.5	1.1	4.8	−0.7	−2.8	3
2016-02-24	501A503	OPD	01:53:25.5	1.1	7.1	−0.2	−1.6	4
		FEG	01:53:27.3	4.0	24.7	+1.5	+9.6	4
2016-02-25	501A503	GOA	23:55:58.2	2.4	8.8	−1.6	−6.0	5
2016-03-04	501A502	GOA	02:09:59.3	2.3	7.7	+1.8	+6.1	6
2016-03-18	501A502	OPD	06:53:17.0	2.5	5.9	+9.7	+22.4	7
2016-04-02	501A502	OPD	05:46:03.2	2.5	7.0	−3.2	−9.2	8
		FOZ	05:45:57.1	2.2	6.4	−9.3	−26.7	8
		FEG	05:45:59.1	3.8	10.8	−7.4	−21.1	8
2016-04-02	501A504	OPD	23:24:20.4	1.2	6.6	−8.1	−44.9	9
		FOZ	23:24:22.4	1.4	7.5	−6.2	−33.9	9
		FEG	23:24:22.3	3.5	19.1	−6.3	−34.5	9
2016-04-12	501A504	OPD	04:35:29.7	8.9	51.6	+5.2	+30.3	10
		FOZ	04:35:31.1	1.1	6.4	+6.6	+38.3	10
		FEG	04:35:29.1	2.5	14.5	+4.7	+27.1	10
2016-04-12	501A502	FOZ	04:45:49.0	10.1	10.5	+19.1	+19.8	11
2016-04-12	502A504	FOZ	05:01:34.6	1.9	11.2	+0.0	+0.1	12
		FEG	05:01:36.1	4.2	25.2	+1.6	+9.8	12
2016-04-12	502A504	OPD	21:17:16.2	0.8	2.9	−7.2	−25.1	13
2016-04-19	501A502	OPD	23:35:15.3	1.0	3.8	−0.1	−0.2	14
		FOZ	23:35:14.2	2.1	8.2	−1.3	−4.8	14
		GOA	23:35:13.3	2.2	8.2	−2.1	−7.8	14
		UTF	23:35:15.2	3.2	12.0	−0.2	−0.6	14
		OHP	23:35:13.9	1.5	5.6	−1.4	−5.5	14
2016-04-20	501A502	OHP	20:15:57.8	1.8	8.7	−3.6	−17.0	15
2016-04-24	502A504	OPD	22:35:12.0	0.5	3.7	−1.5	−11.6	16
		UTF	22:35:13.1	2.6	19.6	−0.4	−3.3	16
2016-04-29	501A503	OPD	00:32:28.1	2.4	16.2	−1.4	−9.2	17
		UTF	00:32:28.6	4.2	28.0	−0.9	−5.8	17
2016-05-02	501A503	OPD	01:08:50.3	1.5	10.5	+0.5	+3.3	18
		FOZ	01:08:50.7	2.3	16.7	+0.8	+6.0	18
		FEG	01:08:49.1	1.8	12.7	−0.7	−4.8	18
		UTF	01:08:51.1	4.5	32.1	+1.3	+9.2	18
2016-05-03	501A503	OPD	01:04:55.4	1.3	4.2	+5.4	+18.2	19
		UTF	01:04:55.5	1.9	6.4	+5.4	+18.4	19
2016-05-06	502A503	OPD	00:59:06.8	6.5	31.6	+3.2	+15.6	20
2016-05-19	502A504	FOZ	22:52:31.9	1.0	6.6	−1.4	−9.1	21
2016-05-27	501A503	FEG	02:00:21.8	5.5	34.2	+0.1	+0.9	22
2016-06-17	502A503	OPD	00:48:02.9	1.3	9.0	−0.3	−2.2	23
		FEG	00:48:07.0	4.8	34.3	+3.8	+26.7	23
2016-06-28	501A502	OPD	23:58:57.1	1.4	6.5	+0.2	+0.8	24
		FEG	23:58:59.0	1.1	5.2	+2.1	+9.7	24
2016-06-29	501A503	OPD	22:36:02.2	0.5	2.9	+1.2	+6.6	25
		FEG	22:36:02.9	1.2	6.7	+1.8	+10.3	25
2016-07-08	501A502	OPD	21:51:35.5	0.6	3.2	+3.0	+14.4	26
		FEG	21:51:32.6	3.3	16.2	+0.0	+0.2	26

The time derivatives of equations (5), (6) and (7) are

$$\Delta\dot{x}_{ij} \simeq (\dot{\alpha}_i - \dot{\alpha}_j)\cos(\delta_m) - (\alpha_i - \alpha_j)\sin(\delta_m)\dot{\delta}_m, \tag{8}$$

$$\Delta\dot{y}_{ij} \simeq \dot{\delta}_i - \dot{\delta}_j, \tag{9}$$

$$\dot{\delta}_m = \frac{\dot{\delta}_i + \dot{\delta}_j}{2}. \tag{10}$$

By deriving equation (4) over time, we obtain

$$\frac{\mathrm{d}s_{ij}}{\mathrm{d}t} = \frac{\Delta x_{ij}\Delta\dot{x}_{ij} + \Delta y_{ij}\Delta\dot{y}_{ij}}{s_{ij}}. \tag{11}$$

Table 3. Central instant: results of the mutual approximation campaign for 2017 and 2018. Note that 501 stands for Io, 502 for Europa, 503 for Ganymede and 504 for Callisto. σt_0 is the central instant error in seconds of time and in mas (using the relative velocity in each event obtained with the ephemeris) and Δt is the comparison between the observation and the ephemeris JUP310 (with DE435) from the JPL in the sense of observation minus ephemeris in seconds of time and in mas. N is a sequential number with time that labels each observed mutual approximation. Time is UTC.

Date (yy-mm-dd)	Event	Observer	t_0 (UTC) (hh:mm:ss.ss)	σt_0 (s)	σt_0 (mas)	Δt_0 (s)	Δt_0 (mas)	N
2017-02-07	502A503	FOZ	04:36:54.1	1.0	7.5	+2.0	+14.4	27
2017-02-26	502A503	FOZ	04:32:43.5	1.3	9.0	+2.6	+17.7	28
2017-02-27	501A502	FOZ	03:36:51.3	1.1	5.7	+3.6	+18.8	29
2017-03-07	501A502	FOZ	03:00:44.4	32.9	31.0	−2.2	−2.1	30
2017-03-14	501A503	FOZ	07:19:33.8	1.1	3.4	+0.9	+2.8	31
2017-04-04	501A503	OHP	20:43:34.4	0.7	6.3	+1.9	+17.9	32
2017-04-06	501A503	FEG	03:46:43.1	2.2	13.1	+3.9	+23.0	33
2017-04-08	501A502	FOZ	01:52:40.5	1.0	7.6	+2.3	+16.9	34
2017-04-13	501A502	FOZ	05:49:28.3	1.0	5.8	+1.8	+10.0	35
2017-05-06	502A503	GOA	02:16:30.2	1.7	12.1	+2.9	+20.9	36
2017-05-08	501A502	FOZ	01:11:26.5	1.0	4.5	+1.2	+5.5	37
2017-05-13	501A503	FOZ	04:47:32.1	1.0	7.0	+1.0	+6.7	38
2017-05-15	501A502	FEG	03:23:43.1	1.7	6.8	+2.0	+8.4	39
2017-05-31	501A503	FEG	22:30:36.2	27.9	14.7	+4.0	+2.1	40
2017-06-08	501A502	GOA	23:48:58.1	1.8	4.3	+2.9	+6.9	41
		FEG	23:48:57.1	7.5	17.6	+1.9	+4.4	41
2017-06-23	501A502	FOZ	23:17:09.0	1.1	2.8	+2.4	+5.7	42
		GOA	23:17:07.7	1.9	4.6	+1.2	+2.9	42
2017-07-06	501A502	FOZ	22:58:42.6	1.4	3.4	+1.0	+2.4	43
		FEG	22:58:41.1	19.4	48.3	−0.5	−1.3	43
2017-07-25	502A503	FOZ	22:40:24.8	1.2	4.9	+2.9	+11.6	44
		FEG	22:40:21.3	3.3	13.1	−0.5	−1.9	44
2017-08-02	501A502	FEG	23:38:20.0	7.7	28.7	+4.8	+17.6	45
2017-08-10	501A502	FOZ	23:41:23.6	48.2	30.6	−1.9	−1.2	46
2017-08-24	503A504	FEG	22:35:37.6	6.6	16.1	+1.4	+3.3	47
2018-03-05	501A502	FOZ	05:10:29.7	0.6	3.7	−0.4	−2.4	48
2018-03-11	501A503	OPD	05:40:46.7	1.8	4.4	+0.3	+0.6	49
		FOZ	05:40:47.0	2.0	5.0	+0.5	+1.3	49
2018-03-12	501A502	OPD	07:20:57.6	0.5	3.0	+0.1	+0.4	50
		FOZ	07:20:58.8	1.4	8.4	+1.2	+7.3	50
2018-03-17	501A502	FOZ	03:15:03.2	0.8	7.0	+0.2	+1.5	51
2018-03-17	502A504	FOZ	03:41:06.1	2.1	13.0	+1.8	+11.1	52
2018-03-24	501A502	FOZ	05:18:47.9	0.7	5.7	+1.4	+11.3	53
2018-04-06	501A502	OPD	02:40:32.0	1.2	8.8	+1.1	+8.2	54
		FOZ	02:40:31.4	1.0	7.7	+1.2	+8.5	54
2018-06-11	502A503	FEG	23:03:46.0	1.8	12.4	−0.4	−3.0	55
		GOA	23:03:45.1	1.2	8.3	−1.3	−9.2	55
2018-06-19	502A503	FOZ	01:55:19.9	1.1	7.6	+0.3	+2.4	56
2018-06-22	501A503	OPD	02:17:12.6	4.5	5.7	−2.0	−2.5	57
		FOZ	02:17:12.5	5.6	7.0	−4.7	−6.0	57
		FEG	02:17:09.5	7.2	9.0	−5.0	−6.3	57
		GOA	02:17:09.9	6.5	8.2	−2.0	−2.5	57
2018-06-23	501A502	FOZ	00:40:47.4	1.1	9.1	−1.9	−16.1	58
2018-07-07	501A503	OPD	00:30:56.8	1.1	6.3	−0.1	−0.8	59
		FEG	00:30:57.0	2.2	12.5	+0.1	+0.4	59
2018-07-11	502A504	OPD	22:48:02.8	1.4	6.7	−0.4	−1.5	60
2018-07-12	501A504	OPD	00:30:30.1	2.5	6.7	−1.2	−3.2	61
2018-07-12	501A502	OPD	01:07:37.4	1.0	5.2	−0.5	−2.5	62
		FEG	01:07:36.3	2.5	12.8	−1.6	−8.1	62
2018-07-13	502A503	OPD	02:01:30.9	1.1	4.4	+0.1	+0.4	63
		FEG	02:01:29.9	5.4	20.9	−0.9	−3.4	63
2018-07-19	501A504	OPD	01:52:08.6	1.9	8.9	−3.4	−16.2	64
		FOZ	01:52:09.3	2.1	10.1	−2.8	−13.4	64
2018-08-07	502A503	OPD	23:15:18.8	1.3	8.1	−1.0	−6.6	65
2018-08-12	501A502	OPD	23:54:58.4	1.1	3.4	−1.2	−3.5	66
		FOZ	23:54:58.5	1.2	3.5	−1.1	−3.3	66

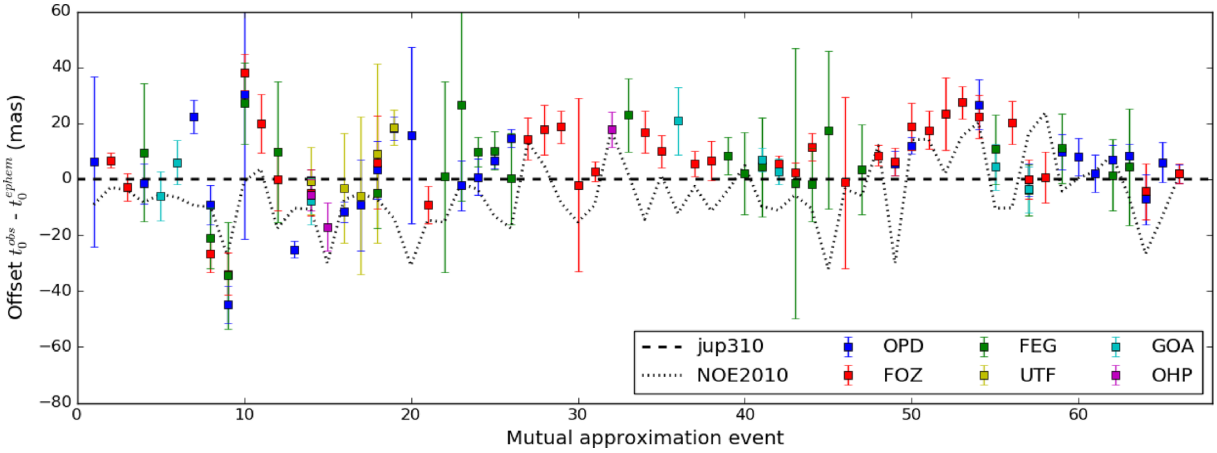

Figure 6. Illustration of the APPROX campaign's results. The *y*-axis is the central instant offset relative to the jup310 ephemeris with DE435 (dashed line at zero offset) and the error bars represent the error of each observation. The *x*-axis is the event's label; each colour represents one site. The dotted line represents the difference between the NOE-5-2010-GAL.a and JUP310 ephemeris with DE435.

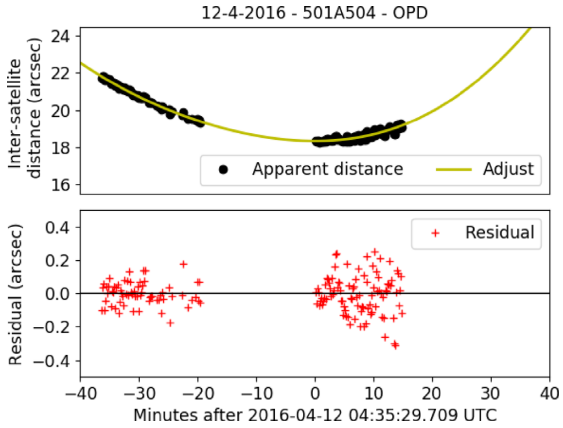

Figure 7. Observed apparent distances in the plane of the sky for Io and Callisto in the mutual approximation of 2016 April 12 seen from OPD. Inter-satellite distances, *d*, are denoted by black dots and the model fit is shown by the yellow line. In the bottom panel, the red crosses are the residual of the fitting. We used the nominal pixel scale (Table 1) to convert the apparent distances from pixels to arcsec. The internal error for this observation was large, 8.9 s of time (51.6 mas), due to the central gap and to the lack of observations 15 min after the central instant.

Then, we derive equation (11) over c_l to obtain

$$\frac{\partial}{\partial c_l}\left(\frac{\mathrm{d}s_{ij}^{c}}{\mathrm{d}t}(t_0)\right) = \frac{1}{s_{ij}}\left[\Delta\dot{x}_{ij}\frac{\partial\Delta x_{ij}}{\partial c_l} + \Delta x_{ij}\frac{\partial\Delta\dot{x}_{ij}}{\partial c_l} + \Delta\dot{y}_{ij}\frac{\partial\Delta y_{ij}}{\partial c_l} + \Delta y_{ij}\frac{\partial\Delta\dot{y}_{ij}}{\partial c_l}\right] - \frac{1}{s_{ij}^{3}}\left(\Delta x_{ij}\Delta\dot{x}_{ij} + \Delta y_{ij}\Delta\dot{y}_{ij}\right) \times\left[\Delta x_{ij}\frac{\partial\Delta x_{ij}}{\partial c_l} + \Delta y_{ij}\frac{\partial\Delta y_{ij}}{\partial c_l}\right]. \quad (12)$$

Therefore, we can write the conditional equation (3) with the use of the explicit form of equation (12).

A similar method has already been tested by Emelyanov (2017) and this has proved to be very efficient when other observations of different types (right ascension, declination, relative distance) are fitted together with the central instants from mutual approximations.

6 CONCLUSIONS

The National Observatory (ON) from Brazil, with the collaboration of the IMCCE (Paris Observatory – France) and Valongo Observatory (UFRJ – Brazil), organized the mutual approximation campaign for the Galilean moons (APPROX). This campaign had the participation of six observational sites and obtained 104 distance curves for 66 events. The central instants obtained had an average internal error of 11.3 mas. The external comparisons gave a rms of 14.4 mas with respect to the JPL JUP310 ephemeris and 18.1 mas with the IMCCE NOE-5-2010-GAL.a ephemeris, using the DE435. About 65 per cent of our results had precision better than 10 mas, 87 per cent better than 20 mas and 91 per cent better than 30 mas. Improvements in the study of the tidal force in the Jovian system require positions with a precision better than 30 mas (Lainey et al. 2009; Lainey 2016).

We used the methane narrow-band filter centred at 889 nm with 15 nm width to reduce Jupiter's scattered light. We remark that the time recorded in the images was carefully corrected by the use of GPS receivers or time calibration software.

The results show that the method of mutual approximations is suitable for small telescopes, which can be used to provide continually high-precision central instants between two satellites.

We also presented a way to fit the observed central instants into dynamical models in order to develop new ephemeris.

The technique of mutual approximations is an alternative high-precision astrometric method that serves to improve the orbits of natural satellites. Unlike mutual phenomena, mutual approximations can be observed at any time independent of the equinox of the host planet. Observational campaigns, such as the one presented here, can increase the accuracy and precision of ephemeris and can be helpful to space missions aimed at the Jovian system, such as

the European Space Agency's mission JUpiter ICy moons Explorer (JUICE)[6] and NASA's mission Europa Clipper.[7]

ACKNOWLEDGEMENTS

This study was financed in part by the Coordenação de Aperfeiçoamento de Pessoal de Nível Superior - Brazil (CAPES) - Finance Code 001. Part of this research is suported by INCT do e-Universo, Brazil (CNPQ grants 465376/2014-2). Based in part on observations made at the Laboratório Nacional de Astrofísica (LNA), Itajubá-MG, Brazil, and at Observatoire de Haute Provence (CNRS), France. BM is grateful for the CAPES/Cofecub-394/2016-05 grant. RVM acknowledges the following grants: CNPq-306885/2013, CAPES/Cofecub-2506/2015, FAPERJ/PAPDRJ-45/2013 and FAPERJ/CNE/05-2015. MA is grateful for the CNPq (Grants 473002/2013-2 and 308721/2011-0) and FAPERJ (Grant E-26/111.488/2013). JIBC acknowledges CNPq grant 308150/2016-3. RS and OCW acknowledge Fapesp proc. 2016/24561-0, CNPq proc 312813/2013-9 and 305737/2015-5. FBR acknowledges CNPq support, process 309578/2017-5. VL's research was supported by an appointment to the National Aeronautics and Space Administration (NASA) Postdoctoral Program at the NASA Jet Propulsion Laboratory, California Institute of Technology, administered by the Universities Space Research Association under contract with NASA.

REFERENCES

Arlot J.-E. et al., 1982, A&A, 111, 151
Arlot J.-E. et al., 2012, A&A, 544, A29
Arlot J.-E. et al., 2013, A&A, 557, A4
Arlot J.-E. et al., 2014, A&A, 572, A120
Assafin M., Vieira Martins R., Camargo J. I. B., Andrei A. H., Da Silva Neto D. N., Braga-Ribas F., 2011, in Tanga P., Thuillot W., eds, Gaia follow-up network for the solar system objects: Gaia FUN-SSO Workshop Proceedings. IMCCE, Paris, p. 85
Butcher E., Stevens R., 1981, News Letter Kitt Peak National Observatory, 16, 6
Charnoz S. et al., 2011, Icarus, 216, 535
Crida A., Charnoz S., 2012, Science, 338, 1196
De Sitter W., 1928, Leiden Ann., 16, 1
Dias-Oliveira A. et al., 2013, MNRAS, 432, 225
Emelyanov N. V., 2009, MNRAS, 394, 1037
Emelyanov N. V., 2017, MNRAS, 469, 4889
Karkoschka E., 1994, Icarus, 111, 174
Karkoschka E., 1998, Icarus, 133, 134
Kiseleva T. P., Izmailov I. S., Kiselev A. A., Khrutskaya E. V., Khovritchev M. Yu., 2008, Planet. Space Sci., 56, 1908
Lainey V., 2016, Celest. Mech. Dyn. Astron., 126, 145
Lainey V., Duriez L., Vienne A., 2004a, A&A, 420, 1171
Lainey V., Arlot J.-E., Vienne A., 2004b, A&A, 427, 371
Lainey V., Arlot J. -E., Karatekin O., Van Van Hoolst T., 2009, Nature, 459, 957
Lieske J. H., 1987, A&A, 176, 146
Lindegren L., 1977, A&A, 57, 55
Morgado B., Assafin M., Vieira-Martins R., Camargo J. I. B., Dias-Oliveira A., Gomes-Júnior A. R., 2016, MNRAS, 460, 4086
Peng Q. Y., Vienne A., Lainey V., Noyelles B., 2008, Planet. Space Sci., 56, 1807
Peng Q. Y., He F., Lainey V., Vienne A., 2012a, MNRAS, 419, 1977
Peng Q. Y., Vienne A., Zhang Q. F., Desmars J., Yang C. Y., He H. F., 2012b, AJ, 144, 170
Robitaille T. P. et al., 2013, A&A, 558, A33
Saquet E. V. et al., 2018, MNRAS, 474, 4730

[6]See http://sci.esa.int/juice/.
[7]See https://www.nasa.gov/europa.

[1]*Observatório Nacional/MCTIC, R. General José Cristino 77, Rio de Janeiro, RJ 20.921-400, Brazil*
[2]*Laboratório Interinstitucional de e-Astronomia - LIneA, Rua Gal. José Cristino 77, Rio de Janeiro, RJ 20921-400, Brazil*
[3]*Observatório do Valongo/UFRJ, Ladeira Pedro Antonio 43, Rio de Janeiro, RJ 20080-090, Brazil*
[4]*Universidade Estadual do Oeste do Paraná (Unioeste), Avenida Tarquínio Joslin dos Santos 1300, Foz do Iguaçu, PR 85870-650, Brazil*
[5]*Polo Astronômico Casimiro Montenegro Filho/FPTI-BR, Avenida Tancredo Neves 6731, Foz do Iguaçu, PR 85867-900, Brazil*
[6]*UNESP - São Paulo State University, Grupo de Dinâmica Orbital e Planetologia, CEP 12516-410, Guaratinguetá, SP 12516-410, Brazil*
[7]*Universidade Federal do Espírito Santo, Av. Fernando Ferrari 514, Vitória, ES 29075-910, Brazil*
[8]*Federal University of Technology - Paraná (UTFPR/DAFIS), Av. Sete de Setembro, 3165, CEP 80230-901 - Curitiba - PR - Brazil*
[9]*Institut Polytechnique des Sciences Avancées IPSA, 63 bis Boulevard de Brandebourg, 94200 Ivry-sur-Seine, France*
[10]*IMCCE, Observatoire de Paris, PSL Research University, CNRS-UMR 8028, Sorbonne Universités, UPMC, Univ. Lille 1, 77 Av. Denfert-Rochereau, 75014 Paris, France*
[11]*Escola SESC de Ensino Médio, Avenida Ayrton Senna, 5677, Rio de Janeiro - RJ, 22775-004, Brazil*
[12]*Jet Propulsion Laboratory, California Institute of Technology, 4800 Oak Grove Drive, Pasadena, CA 91109-8099, USA*

This paper has been typeset from a TEX/LATEX file prepared by the author.